AIAA SciTech Forum
6-10 January 2020, Orlando, FL
AIAA Scitech 2020 Forum

10.2514/6.2020-1060

Numerical Investigation of Coflow Jet Active Flow Control 3D Swept Cylinders

Jeremy Boling*,Yunchao Yang†,Ge-Cheng Zha‡
Department of Mechanical and Aerospace Engineering
University of Miami, Coral Gables, Florida 33124
E-mail: gzha@miami.edu

Cale Zeune§
Aerodynamic Technology Branch,
Aerospace Systems Directorate, AFRL/RQVA
Wright-Patterson AFB, Ohio 45433

This paper studies aerodynamic force enhancement and flight control using Co-Flow Jet (CFJ) active flow control for 3D swept cylinders. The application background is to replace the V-tail control surface for aerial refueling boom. Past studies show the ability for CFJ actuated cylinders to outperform potential flow predictions of maximum lift. This study applies similar methodology to higher Mach flows and 3D swept cylinders in order to control the motion of the cylinder. The CFD simulations employ a validated RANS solver with one-equation Spalart-Allmaras turbulence modeling. The inviscid fluxes are discretized with a 3rd order WENO scheme, and the viscous terms are discretized with 2nd order central differencing. With Mach numbers of 0.25 for a 2D cylinder, a lift coefficient of 10.6 is achieved with substantially lower power consumption than the previous study. The 2D CFJ cylinder configuration is then used to create the 3D swept cylinder. Similarly, a 3D cylinder swept at 60 degrees with an aspect ratio of 10, the study purpose is two fold: 1) side force enhancement by CFJ for lateral motion control; 2) Side force cancellation by CFJ to enhance the pitching moment for longitudinal control. By applying a set of CFJ flow control for 15% of the cylinder span, a very large side force coefficient of 3 is achieved. It is more than required to control the cylinder lateral motion. By using two sets of CFJ oriented in opposing injecting directions, the side force can be canceled out, while enhancing the pitching moment for longitudinal control. The CFJ injection and suction slot location affect the direction of the resultant force vector. CFJ active flow control can be manipulated to vector the aerodynamic force on the CFJ cylinder. This study indicates that it is feasible to control a 3D swept cylinder lateral and longitudinal motion using CFJ without a V-tail control surface. However, the study is just a initial step. More detailed CFJ and configurations design iteration are necessary with wind tunnel testing to validate the flight control features.

Nomenclature

V	Flow Velocity
ρ	Air Density
α, AoA	Angle of Attack
$\dot{m}$	Mass Flow Rate
M	Mach Number

*Graduate Research Assistant
†Postdoc at University of Florida
‡Professor, AIAA Associate Fellow
§Chief Engineer

M_i	Isentropic Mach Number
Re	Reynolds Number
L	Aerodynamics Lift
D	Aerodynamic Drag
p	Static Pressure
p_0	Total Pressure
η	Pumping Power
q_∞	Freestream Dynamic Head, $\frac{1}{2}\rho_\infty {V_\infty}^2$
C_L	Lift Coefficient, $\frac{L}{q_\infty S}$
C_{LMAX}	Maximum Lift Coefficient
C_D	Drag Coefficient, $\frac{D}{q_\infty S}$
C_M	Moment Coefficient, $\frac{M}{q_\infty S c}$
C_p	Pressure Coefficient, $\frac{p-p_\infty}{q_\infty}$
C_μ	Jet Momentum Coefficient, $\frac{\dot{m}_j v_j}{q_\infty S}$
$(\frac{L}{D})$	Conventional Aerodynamic Efficiency
P_c	Power Coefficient, $\frac{L}{q_\infty S V_\infty}$
∞	Free Stream Conditions
j	Jet Conditions

I. Introduction

I.A. Background

Flows around cylinders are widely encountered in various industry applications such as the pipes in deep sea drilling, bridge suspension cables and bridge pylons, aerial refueling booms, etc. The flows are inherently unstable and vortical with vortex shedding. The instability of the cylinder flows may affect the functioning of the system and even damage it. For aerial refueling booms, high precision is required to control the motion of the booms between the tanker and the recipient aircraft. A rigid refueling boom typically uses two lifting surfaces in an H-tail or V-tail configuration for flight control, which requires complex and heavy hydraulic systems. An active flow control that can replace the tail configuration control surfaces for cylindrical refueling booms is desirable.

The Kutta-Joukowski theorem in aerodynamics has been fundamental for understanding force from a circulation perspective. When applied to a cylinder, the basic concept of physically rotating a cylinder to create lift has demonstrated the concept for a century. Figure 1 shows the flow around a rotating cylinder. Increasing the circulation moves the stagnation points closer together.

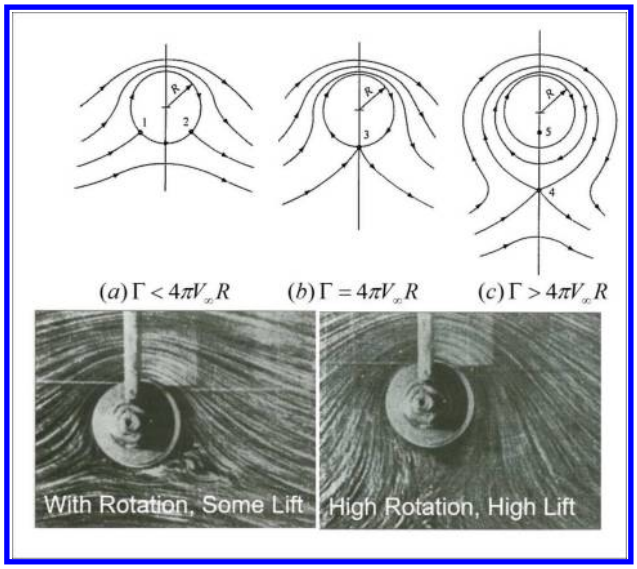

Figure 1: Rotating Cylinder Flow Control adapted from Anderson[1]

Equations 1, 2, and 3 describe the Kutta-Joukowski lift theorem for a cylinder. In essence, a vortex around a cylinder creates an induced flow in the direction of the freestream along the top of the cylinder, and against the direction of flow along the bottom of the cylinder. The viscous boundary layer entrains the incoming flow in the direction of the vortex which is, in the classical case as indicated in Figure 1, clockwise. The flow above the cylinder is assisted by the induced flow, while below the cylinder is opposed by the induced flow. By integrating the surface pressure over the entire cylinder, a net lifting force can be calculated. It can be seen that the strength of the circulation is dependent on the tangential velocity of the spinning cylinder.

$$L = \rho G V_\infty \tag{1}$$

$$G = 2\pi b V_r \tag{2}$$

$$V_r = 2\pi b s \tag{3}$$

Rotating a mechanical cylinder system at high speeds to compensate for increased freestream velocities will have large energy requirements. Due to inertia, circulation cannot be controlled quickly when using a rotating cylinder, as changes in angular velocity are not instantaneous. For this reason, it is desirable if an active flow control can enhance the lift without mechanically rotating the cylinder. Yang and Zha demonstrate that the coflow jet (CFJ) active flow control can achieve this purpose.[2]

I.B. CFJ Active Flow Control

The Co-Flow Jet airfoil is a zero-net mass-flux(ZNMF) active flow control technique developed by Zha and his team.[3–16] Applying this technique to a traditional airfoil provides the ability to increase lift and aerodynamic efficiency at low energy expenditure. This low energy expenditure results from placing an injection slot near the leading edge and a suction slot near the trailing edge. Flow is injected near the suction peak and sucked in at a position of higher pressure. Applied to a cylinder, these locations resemble Figure 2. With the help of a micro-compressor pumping system inside the cylinder, a small amount of air is sucked in from the suction slot and the energized flow is injected through the injection slot in the direction tangent to the main flow. The process does not add any mass flow and hence is a ZNMF system. This technique works by energizing the boundary layer and hence increasing circulation, augmenting lift while decreasing pressure drag due to enhanced leading edge suction and filled wake.

The purpose of this paper is to apply the CFJ active flow control to 3D swept cylinders to mimic an aerial refueling boom. The goal is to generate the required force and moment to move the boom without using V-tail control surface. It has the potential advantage to reduce the weight of the refueling boom and its aerodynamic drag when it is stowed. The focus of this study is two fold: 1) side force enhancement by CFJ for lateral motion control; 2) Side force cancellation by CFJ to enhance the pitching moment for longitudinal control.

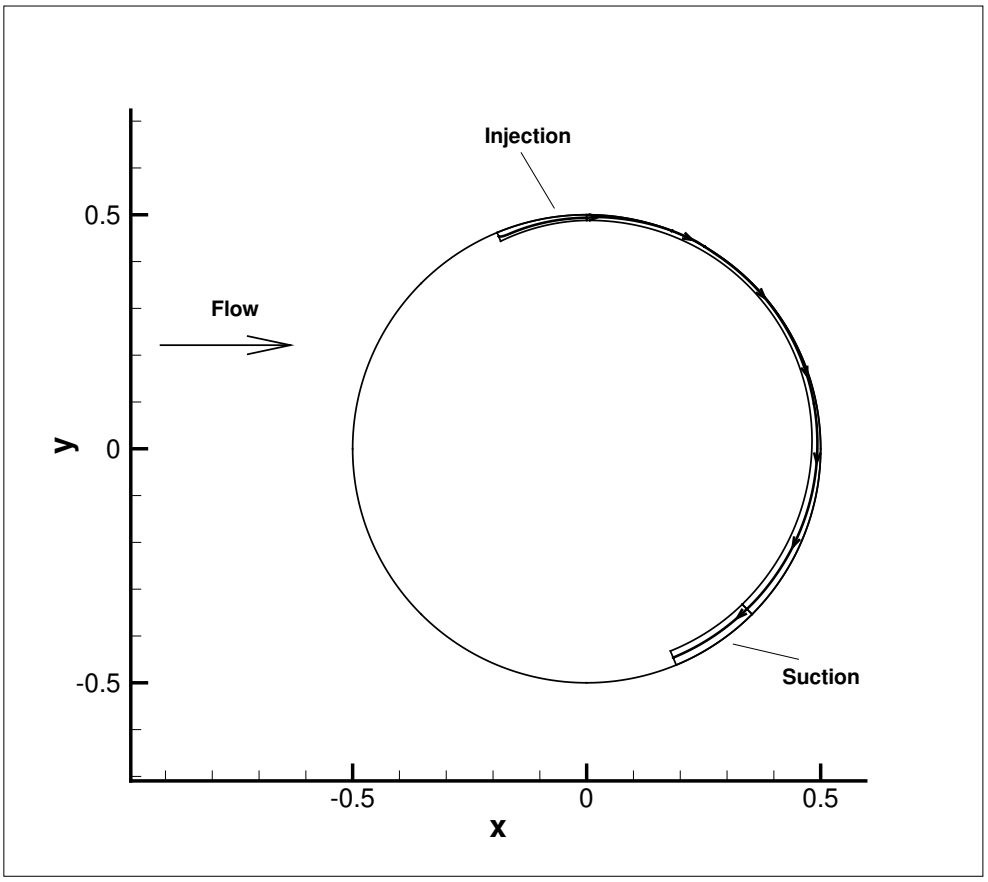

Figure 2: The sketch of a baseline airfoil and a CFJ airfoil.

II. Methodology

II.A. Numerical Approach

The in-house computational fluid dynamics(CFD) code Flow-Acoustics-Structure Interaction Package(FASIP) is utilized to conduct the numerical simulations. The Reynolds averaged Navier-Stokes(RANS) equations with one-equation Spalart-Allmaras(SA)[17] turbulence model is used for this research. The low diffusion E-CUSP scheme suggested by Zha et al.[18] with the 3rd order weighted essentially non-oscillatory(WENO) scheme is utilized to evaluate the inviscid fluxes. The 2nd order central differencing method is used for the viscous terms discretization. The implicit Gauss-Seidel(GS) line relaxation with two alternative sweeping direction in each time step is applied to achieve a fast convergence rate.[19] Parallel computing is implemented to save wall clock simulation time.[20] The code is extensively validated with various CFJ flows.[7, 14, 20–23]

II.B. CFJ Airfoil Parameters

II.B.1. Drag and Lift

Zha et al.[5] give the following formulations to calculate the lift and drag due to CFJ effect for CFD simulation

$$R_x = (\dot{m}_j V_{j1} + p_{j1} A_{j1})\ cos(\theta_1 - \alpha) - (\dot{m}_j V_{j2} + p_{j2} A_{j2})\ cos(\theta_2 + \alpha) \tag{4}$$

$$R_y = (\dot{m}_{j1} V_{j1} + p_{j1} A_{j1})\ sin(\theta_1 - \alpha) + (\dot{m}_{j2} V_{j2} + p_{j2} A_{j2})\ sin(\theta_2 + \alpha) \tag{5}$$

where x and y represent the drag and lift direction respectively, subscripts 1 and 2 stand for the injection and suction, θ_i $(i = 1, 2)$ is the angle between the injection or suction slot surface and the line normal to the airfoil chord, and α is the AoA, as shown in Figure 3.

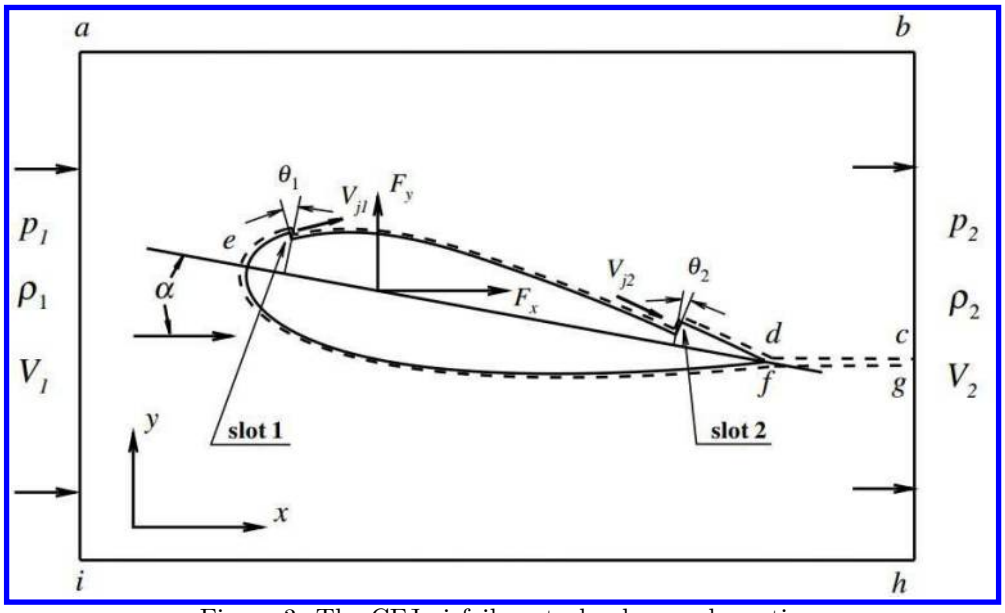

Figure 3: The CFJ airfoil control volume schematic.

The total drag and lift of the CFJ airfoil can then be expressed as below

$$D = F_x - R_x \tag{6}$$

$$L = F_y - R_y \tag{7}$$

where F_x and F_y are the drag and lift force due to surface integral of pressure and shear stress. The corresponding drag and lift coefficients are expressed as following

$$C_D = \frac{D}{\frac{1}{2}\rho_\infty {V_\infty}^2 S} \tag{8}$$

$$C_L = \frac{L}{\frac{1}{2}\rho_\infty {V_\infty}^2 S} \tag{9}$$

where ρ_∞ and V_∞ denote the free stream density and velocity. S is the wing planform area. For 2-D airfoil study, S denotes the planform area per unit span, which is equal to the airfoil chord length.

II.B.2. Jet Momentum

The jet momentum coefficient C_μ is a parameter used to quantify the jet intensity, which is defined as

$$C_\mu = \frac{\dot{m} V_j}{\frac{1}{2}\rho_\infty {V_\infty}^2 S} \tag{10}$$

where $\dot{m}$ is the injection mass flow rate, V_j is the averaged injection velocity at the injection slot opening.

II.B.3. Power Consumption

The CFJ can be implemented by mounting a pumping system inside the wing that withdraws air from the suction slot and blows it into the injection slot. The power consumption can be determined by the jet mass flow and total enthalpy change as follows

$$P = \dot{m}(H_{01} - H_{02}) \tag{11}$$

where H_{01} and H_{02} are the total enthalpy in the injection cavity and suction cavity, respectively. P is the power required by the pump. Introducing the pump efficiency η and total pressure ratio of the pump $\Gamma = \frac{P_{01}}{P_{02}}$, the power consumption can be expressed as

$$P = \frac{\dot{m} C_p T_{02}}{\eta}(\Gamma^{\frac{\gamma-1}{\gamma}} - 1) \tag{12}$$

where γ is the specific heat ratio for air. The power consumption can be further normalized as a power coefficient

$$P_c = \frac{P}{\frac{1}{2}\rho_\infty V_\infty^3 S} \tag{13}$$

II.B.4. Aerodynamic Efficiency

The conventional airfoil aerodynamic efficiency is defined as

$$(\frac{L}{D}) = \frac{C_L}{C_D} \tag{14}$$

For the CFJ airfoil, the ratio above represents the pure aerodynamic relationship between lift and drag. Taking into account the energy consumption of the CFJ, the conventional aerodynamic efficiency is modified by converting the power consumption into a corresponding drag force. The equation of the corrected aerodynamic efficiency is given as follows[10]

$$(\frac{L}{D})_c = \frac{L}{D + \frac{P}{V_\infty}} \tag{15}$$

in which the pump power consumption P is converted into a force $\frac{P}{V_\infty}$ added to the aerodynamic drag D. The formulation above can be further expressed using the non-dimensional coefficients C_L, C_D and P_c as

$$(\frac{L}{D})_c = \frac{C_L}{C_D + P_c} \tag{16}$$

Note that when the pumping power is set to 0, $(\frac{L}{D})_c$ returns to conventional aerodynamic efficiency definition.

III. Results and Discussions

III.A. Mesh and Boundary Conditions

We conduct the 2D simulation first to seek the optimal configuration for a 3D swept cylinder. The 2D CFJ grid features an O-mesh topology. There are 1601 grid points around the circumference of the cylinder with 121 points normal to the wall as listed in Table 1. This gives 216,000 total cells. The far-field boundary is located at 60 diameters. Near the wall the y^+ value is less than 1. This is the same mesh as used by Yang et al. [2] The mesh refinement study indicates that the solution is converged based on the mesh size.

Table 1: Mesh Dimensions for 2D Cylinder

ξ Direction	η Direction	Cell Number
1601	121	216000

The 2D Free-stream of M=0.25 and $Re = 2.2 \times 10^6$ are used in this study. The 3D study is based on a potential wind-tunnel setup and is set to the freestream conditions of M=0.45 and $Re = 2.17 \times 10^6$.

A no slip-boundary condition is imposed on the surface of the cylinder. The inlet half of the O-mesh has a fixed total pressure boundary condition. The outlet of the mesh has a fixed static pressure boundary condition. The 3D mesh is an extrusion of the 2D mesh along the swept cylinder, in order to preserve fidelity and resolve the same flow structures as seen in the 2D analysis. For the 3D simulations, there are two configurations and the associated boundary conditions: 1) Using periodic boundary condition in the spanwise direction to focus on the CFJ effect on side force enhancement and cancellation. For this case, the domain simulated is a part of the cylinder with infinite span. 2) A finite span cylinder with the root imposed with the zero gradient BC around the cylinder and symmetric away from the cylinder. The cylinder tip is meshed to the far field boundary 20 diameters away. This case is set up to have the side force canceled with the pitching moment enhanced about the pivot located at the root. The root boundary condition treatment allows some cross-plane flow as the swept cylinder induces some span-wise flow at the root location.

III.B. CFJ Injection Slot Size and Location Study

The CFJ injection location is determined by the azimuth angle, α_1, given from the top of the cylinder, as show in Figure 4. Suction location is similarly determined by α_2. Injection slot size is based on percentage of cylinder diameter and ranges from 0.9%D to 3%D. To match the injection slot size, the CFJ cylinder suction surface translation (SST) is made to match the injection slot. Since the SST is fixed, some manual shaping of the suction surface is required to blend the injection and suction slot with the rest of the cylinder.

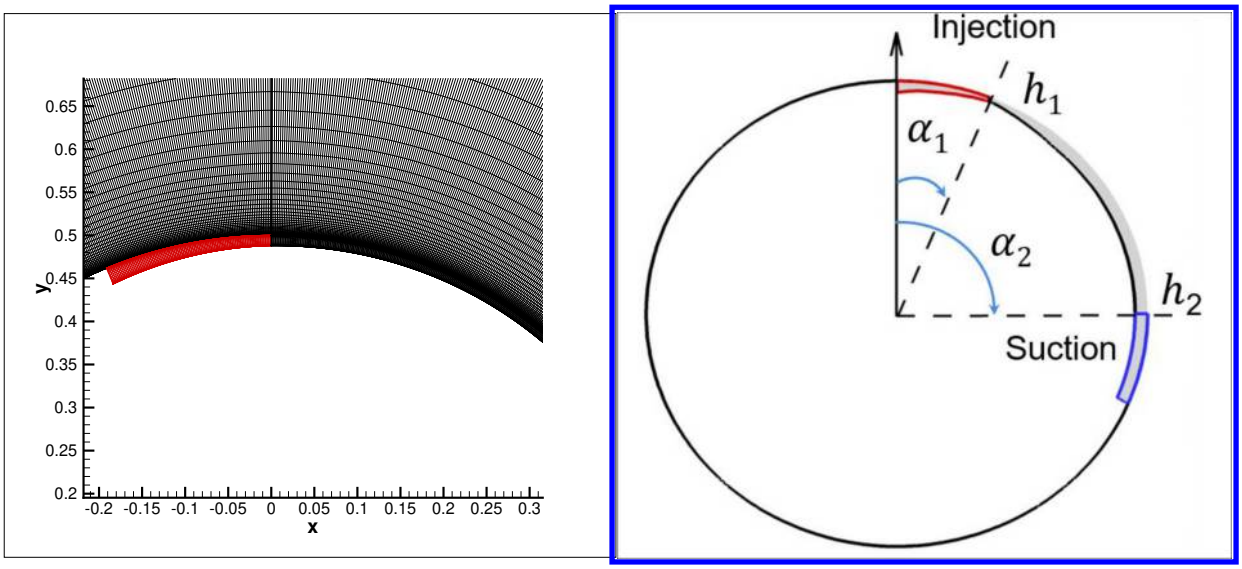

Figure 4: Mesh Example, Injection Size 1.2% at $\alpha_1 = 0°$ (left).

Figure 4 displays an example of the cylinder mesh with injection at $\alpha_1 = 0$. This structured mesh has very dense cell-spacing near the wall, which grows out into the far-field of 60 diameters.

III.C. 2D CFJ Cylinder Study

Previous CFJ cylinder studies are at Mach 0.06 with a very small injection slot size,[2] which is to prove the concept of CFJ cylinder lift enhancement. The injection slot size determining the CFJ power consumption is not studied by Yang, et al.[2] Slower freestream conditions require less momentum to turn the flow. This allows the stagnation point to be completely detached from the cylinder surface as the flow is turned over 180° around the cylinder. Increasing the freestream conditions to Mach 0.25 presents a more difficult challenge since the flow may become transonic with possible shock appearance. As listed in Table 2, the injection and suction location and slot size are varied to seek the optimal configuration with maximum lift enhancement and minimum power consumption.

Table 2: 2D Cylinder Study Parameters

Case	α_2 (°)	Suc Size (% D)	α_1 (°)	Inj Size (% D)	C_μ	C_l	C_d	P_c	C_L/P_c
CFJ-CY-1	135	2	0	1.2	0.3	10.05	0.1447	0.4111	24.46
CFJ-CY-2	135	2.5	0	0.9	0.3	10.18	0.1757	0.6388	15.94
CFJ-CY-3	135	2.5	0	1.2	0.25	8.73	-0.0556	0.2717	32.16
CFJ-CY-4	135	2.5	0	1.2	0.3	10.44	0.1715	0.4138	25.24
CFJ-CY-5	135	2.5	0	1.2	0.35	10.46	0.1565	0.5803	18.03
CFJ-CY-6	135	2.5	22.5	1.2	0.5	10.66	0.1671	1.6816	6.34
CFJ-CY-7	135	2.5	22.5	1.2	0.6	10.56	0.1711	2.2659	4.66
CFJ-CY-8	135	2.5	45	1.2	0.3	10.66	0.1999	0.4254	25.07
CFJ-CY-9	135	2.5	45	1.2	0.5	11.02	-0.0186	1.4430	7.64
CFJ-CY-10	135	2.5	0	2	0.4	9.69	0.1320	0.3168	30.61
CFJ-CY-11	135	2.5	0	2	0.5	10.60	0.3690	0.6662	15.91
CFJ-CY-12	135	2.5	0	2	0.6	10.66	0.3357	1.0359	10.30
CFJ-CY-13	135	2.5	22.5	2	0.5	10.81	0.1761	0.6720	16.10
CFJ-CY-14	135	2.5	22.5	2	0.7	10.69	0.1635	1.2374	8.64
CFJ-CY-15	135	3.5	22.5	3	0.6	9.50	0.0784	0.3157	30.10
CFJ-CY-16	135	3.5	22.5	3	0.77	10.91	0.2048	0.8513	12.82
CFJ-CY-17	135	3.5	22.5	3	0.9	10.79	0.1724	1.2939	8.34

Figure 5 shows a typical steady state cylinder flow with massive flow separation behind the cylinder. An unsteady simulation would show vortex shedding. Steady-state is adequate for this study, as a CFJ cylinder flow is designed to be mostly attached.

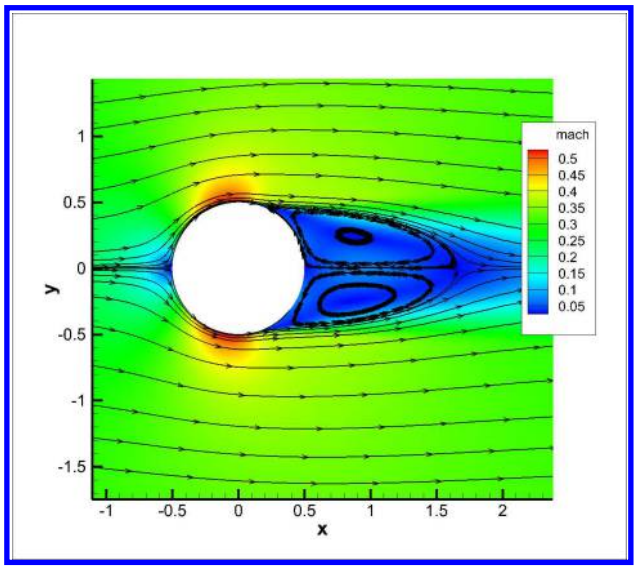

Figure 5: 2D Baseline Cylinder, Mach 0.3

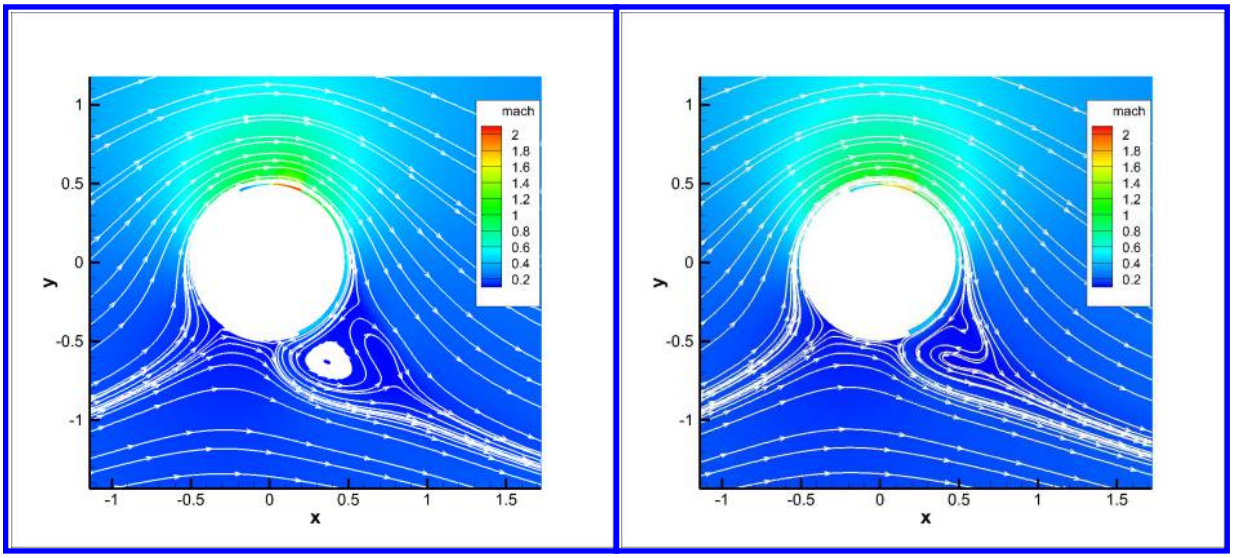

Figure 6: 2D CFJ Cylinder Mach contours, left: Case CFJ-CY-2; right: Case CFJ-CY-4.

Figure 6 shows the Mach contours and streamlines of the Case CFJ-CY-2 (left) and CFJ-CY-4 (right) at C_μ of 0.3. The Case CFJ-CY-2 has a smaller injection size of 0.9%D. The flow has a minor separation near the suction slot. When the injection slot size is increased to 1.2%D, the flow separation is basically removed as shown in Figure 6 for the Case CFJ-CY-4. The larger slot size has a higher CFJ mass flow rate and lower injection jet velocity, which also yields a lower CFJ power coefficient. This is an important result to be used as a potential candidate for the 3D configuration. The overall separation behind the cylinder for the two cases is substantially reduced compared with that of the baseline case. It can also be seen that the stagnation points are moved to the lower half of the cylinder on both the leading and trailing sides. Since there is increased circulation and flow turning, the maximum Mach approaches supersonic conditions. Figure 7 indicates the supersonic flow over the top of the cylinder is terminated by a normal shock for the Case CFJ-CY-6. Moving the injection slot downstream to $\alpha_1 = 45°$ for Case CFJ-CY-6 avoids the shock interacting with the jet directly to reduce the energy loss.

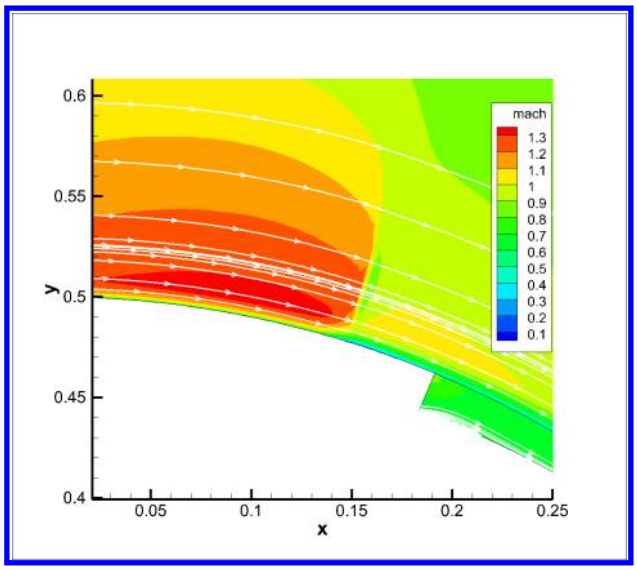

Figure 7: Shockwave, 2D CFJ Cylinder Mach contours, Case CFJ-CY-8

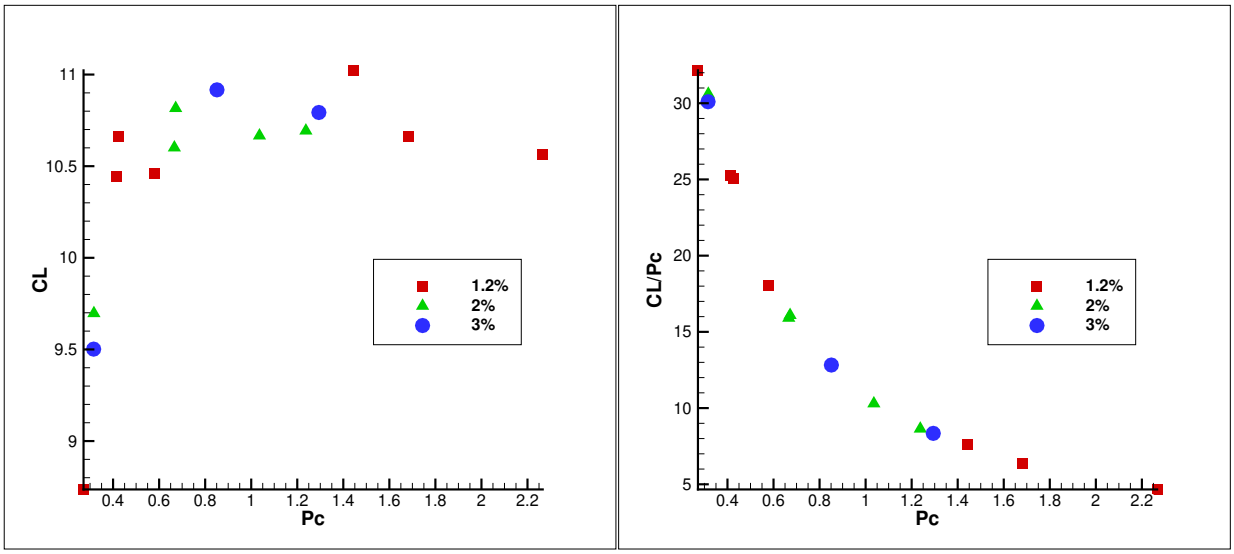

Figure 8: 2D CFJ Cylinder Mach 0.25, Injection Size 1.2%-3%, α_1 = 0°-45°,C_μ = 0.1 – 0.9

Figure 8 shows the lift coefficient C_L vs power coefficient P_C. The maximum C_L of about 11 is obtained by CASE CFJ-CY-9 with the injection slot size of 1.2%D and a power coefficient of 1.5. The Case CFJ-CY-16 with a 3%D injection slot size achieves a similar C_L of 10.92, but the P_C is only 0.9, a 40% reduction. As indicated by Wang and Zha,[24] a larger injection size reduces the CFJ power by using more mass flow rate and lower pressure ratio. Active flow control power is determined linearly by the mass flow rate and exponentially by the pressure ratio. A slot size of 1.2%D demonstrates a high efficiency while still providing high lift. When compared to other configurations, Figure 8 shows that the Case CFJ-CY-8 with an injection slot size of 1.2%D is able to achieve a C_L/P_c of 25. Figure 9 shows the flow-field of this high efficiency configuration. The lift coefficient is 10.6. This will be used as the configuration to construct the 3D swept cylinder. The selection of Case CFJ-CY-8 with a 1.2%D injection slot size configuration is a compromise between the power consumption and the mass flow rate capacity that our ongoing micro-compressor design can provide.

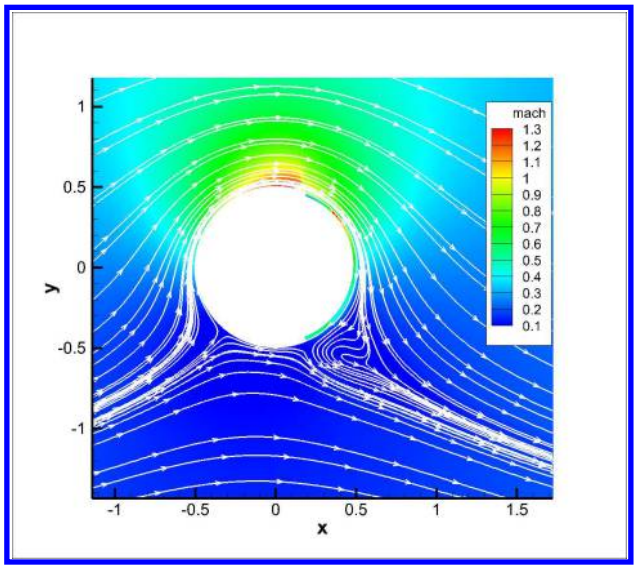

Figure 9: 2D CFJ Cylinder Mach 0.25, 1.2% Injection, 2.5% Suction, Cmu = 0.3, Injection at 45°

III.D. 3D Swept CFJ Cylinder Study

After the 2D CFJ cylinder configuration trade study, CFJ swept cylinders are simulated to mimic the aerial refueling boom. A sweep angle of 60° and a freestream Mach number of 0.45 are used as a potential wind tunnel testing condition.

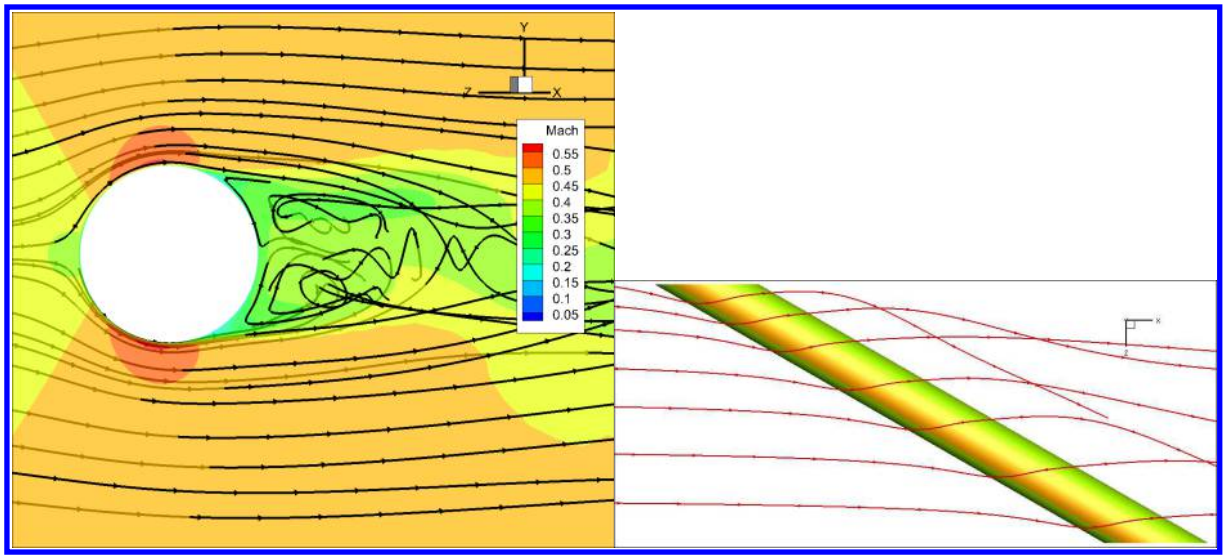

Figure 10: 3D Baseline Cylinder Mach 0.45, 60° Sweep

Figure 10 shows the baseline swept cylinder with an aspect ratio of 10 simulated using the periodic boundary condition in the spanwise direction. The plot on the left in Figure 10 is a cross section displaying Mach contours with streamlines. The flow is separated as expected. The stagnation point is at the leading edge of the cylinder. Viewing the entire cyilnder from its side shows the 3D streamlines are also swept with the cylinder.

The 2D configuration of Case CFJ-CY-8 is used as a starting point for the 3D CFJ cylinder. the mesh is extruded into a swept cylinder. The Case CFJ-CY-8 has an injection slot size of 1.2%D and the location at α_1 of 45° and α_2 of 135° . It provides the nearly highest lift coefficient and a low power coefficient. An increased slot size of 2% is also used to compare the power coefficient values.

III.D.1. Side Moment/Force Generation

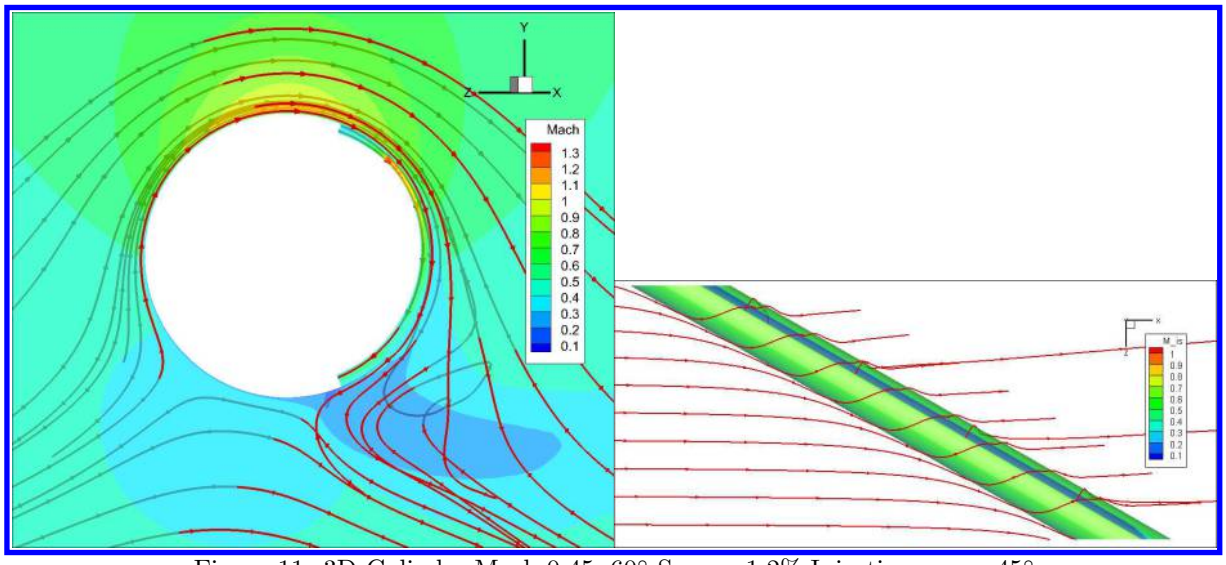

Figure 11: 3D Cylinder Mach 0.45, 60° Sweep, 1.2% Injection, $\alpha_1 = 45°$

Figure 11 shows 3D Mach contours and the streamlines of the CFJ swept cylinder and the cylinder cross-section flow at mid-span. The 3D CFJ cylinder has an aspect ratio of 10 and is simulated using periodic boundary condition along the span. The stagnation points resemble the 2D CFJ cylinder and are moved toward the lower bottom due to the high circulation. . The peak Mach number is also supersonic. The flow separation is basically removed with some minor vortical flow near the suction slot location. Table 4 lists the 3D cases studied. Almost all the cases has α_1 fixed at 45° except the Case 3D-CFJ-CY-8, which has the injection slot at α_1 of 22°. All the suction slot location is at α_2 of 135° except the Case 3D-CFJ-CY-9, which has the α_2 of 180°. The three force coefficients in Table 3, C_X, C_Y, and C_Z represent the force in the direction of streamwise, spanwise and vertical. C_F is the resultant force coefficient determined by Eq. (17). The spanwise force C_Y, which is normal to the incoming flow and pointing into the paper, is the most significant force corresponding to the "lift". The area used to calculate the force coefficient is the planform area of the 3D cylinder, which is equal to the cylinder diameter multiplied by its length. Table 3 indicates that while the Case 3D-CFJ-CY-4 with the 1.2% injection slot size gives the highest overall resultant force, it also requires the highest power coefficient. Similar resultant forces are achieved with 2% slot size. Moving the injection location, α_1, to 22° does not attach the flow better. The resultant force vector indicates much smaller components. Moving the suction slot to $\alpha_2 = 180°$ leads to worse performance.

$$C_F = \sqrt{C_X^2 + C_Y^2 + C_Z^2} \tag{17}$$

Table 3: 3D Swept Cylinder 1.2%-2% Injection Size

Case	$\alpha_1(°)$	$\alpha_2(°)$	Inj Size	Suc Size	P_c	C_μ	C_x	C_y	C_z	C_F
Baseline	-	-	-	-	0	0	0.0650	0.0000	-0.0831	0.1055
3D-CFJ-CY-1	45	135	1.20%	2.50%	0.1427	0.1000	0.0794	2.2514	-0.3200	2.2754
3D-CFJ-CY-2	45	135	1.20%	3.50%	0.0306	0.0500	0.0436	1.0447	-0.1669	1.0588
3D-CFJ-CY-3	45	135	1.20%	3.50%	0.1145	0.1000	0.0651	2.0072	-0.2350	2.0220
3D-CFJ-CY-4	45	135	1.20%	3.50%	0.2935	0.1500	0.0254	3.3961	-0.2315	3.4041
3D-CFJ-CY-5	45	135	2.00%	3.50%	0.0230	0.0500	0.0494	0.8074	-0.2172	0.8375
3D-CFJ-CY-6	45	135	2.00%	3.50%	0.1098	0.1000	0.0624	1.5553	-0.2422	1.5753
3D-CFJ-CY-7	45	135	2.00%	3.50%	0.1228	0.1510	0.0553	2.5485	-0.2710	2.5635
3D-CFJ-CY-8	22	135	1.20%	3.50%	0.0396	0.0500	0.0485	0.8001	-0.0579	0.8037
3D-CFJ-CY-9	45	180	1.20%	3.50%	0.0603	0.0500	0.0605	0.1682	-0.0953	0.2025

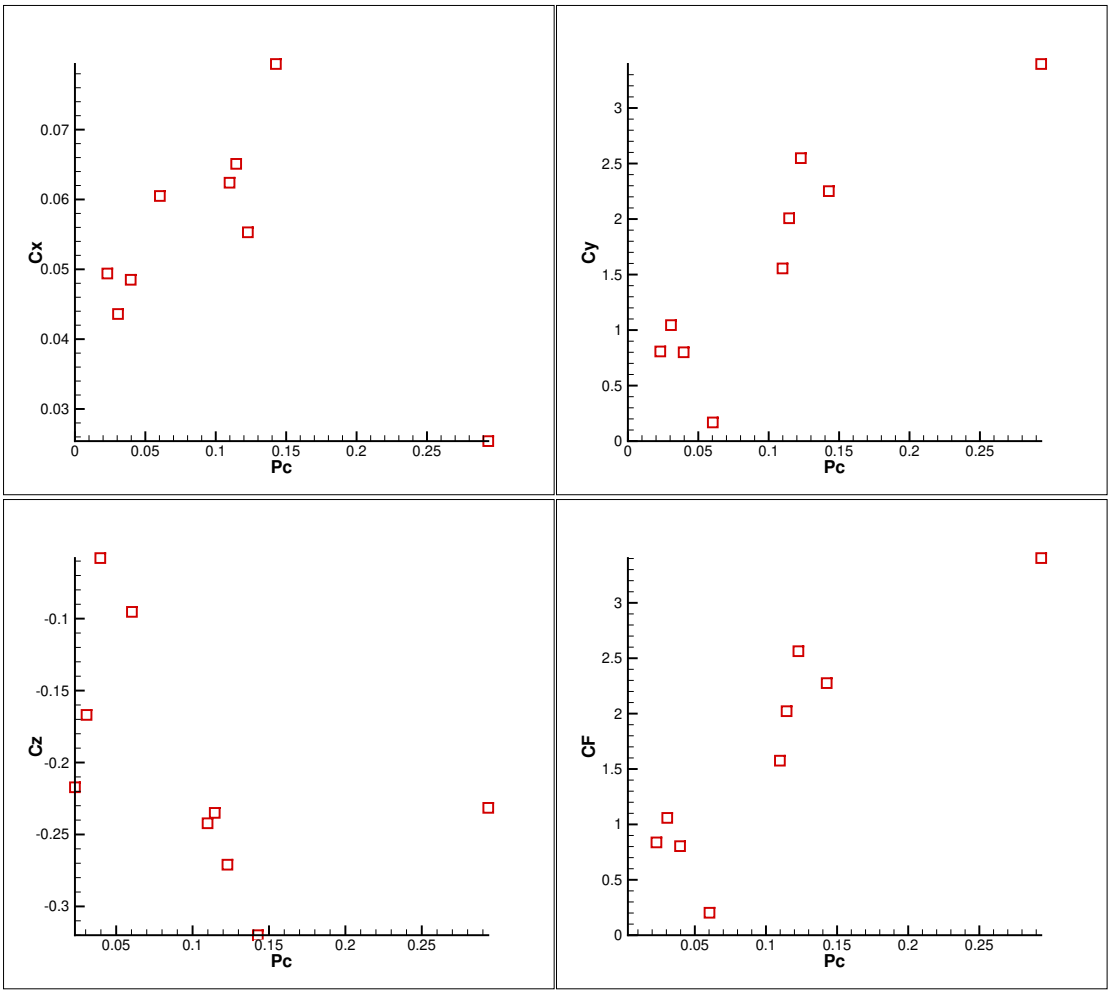

Figure 12: 3D Cylinder C_l v P_c: Injection size 1.2%-2%, Location 0° to 45°, Mach 0.45, 60° Sweep

Figure 12 shows all the coefficients of the component forces and the resultant force vs power coefficient P_C for all the configurations studied. Our primary interest is the side force (C_Y) for the refueling boom lateral motion control. C_Y shows a near linear trend with the CFJ power coefficient.

Table 3 and Figure 12 indicate that the baseline cylinder has no side force due to the symmetry of the cylinder. However, the CFJ controlled cylinder is very effective to generate a large side force (C_Y). A lift (C_Y) coefficient of 2 or 3 in Figure 12 will generate far more than required side force and moment for refueling boom lateral motion control. Table 3 also shows that the vertical force C_Z is substantially increased compared with the baseline cylinder, whereas the drag remains about the same as that of the baseline cylinder.

Figure 13 shows the resultant force coefficient vs the injection jet momentum coefficient. At the same C_μ, the smaller injection slot size results in a higher lift coefficient. This is because the mass flow rate is lower and the jet velocity is higher. It comes with a price that the power coefficient is also higher.

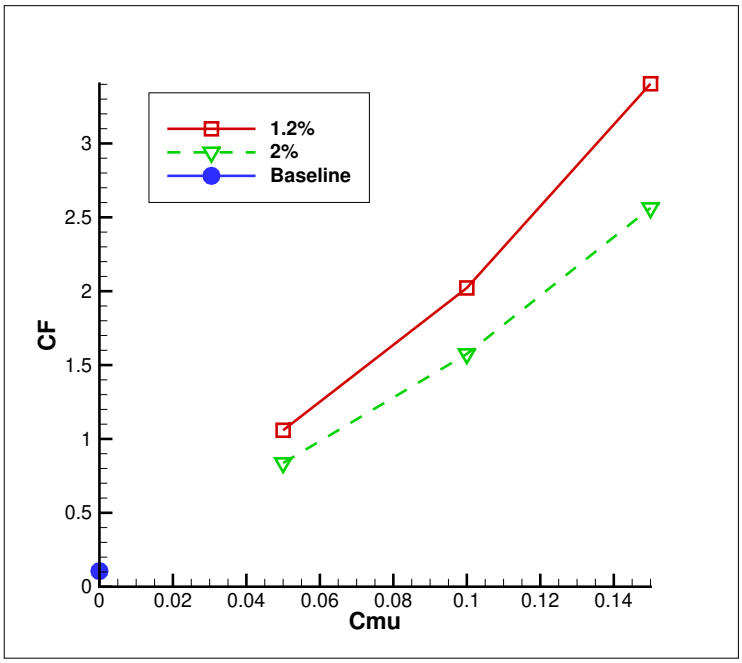

Figure 13: 3D Cylinder Resultant Force Coefficient Mach 0.45, 60° Sweep

III.D.2. Side Force Cancellation

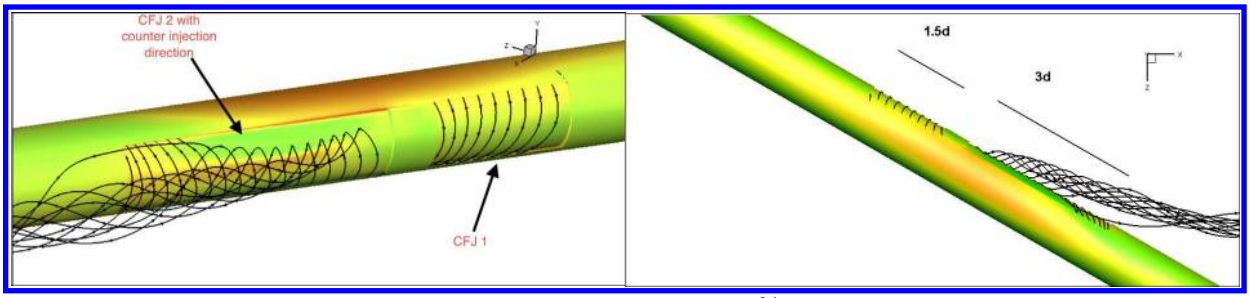

Figure 14: 3D Cylinder Diagram, 2 Injection Slots, 45% Span, Alternating Directions

With the sufficient side force/moment generated by CFJ for lateral motion control presented in the last section, the next requirement to achieve full refueling boom control is to generate sufficient pitching moment. Assuming the pivot of the refueling boom is at the upper end, the vertical force (C_Z) and drag (C_X) will both contribute to the pitching moment.

The requirement for CFJ cylinder pitching motion control is to have little side force, but a large vertical force (C_Z) and drag to generate the required pitching moment. As shown in the last section, applying a CFJ flow control in a part of the CFJ cylinder span will enhance the side force in one direction. The strategy to cancel the side force is to then apply a CFJ with the opposite jet direction in another part of the cylinder span to generate the side force in the opposite direction.

Figure 14 shows the two counter injection CFJ spanning a total of 45% of the cylinder, separated by 5% length. The upstream CFJ 1 spans 15% of the cylinder, and the down stream CFJ 2 has the span size doubled with the jet injecting in the direction opposite to the CFJ 1 injection. Both CFJs have the same injection jet momentum coefficient, C_μ, of 0.05.

Table 4 indicates that most of the side-force (C_Y) is nearly canceled out by the two counter injecting CFJs. Compared with the baseline cylinder, the vertical force component C_Z is increased by 122% and the drag C_X is increased by 48%. Both enhanced C_Z and C_X will increase the pitching moment. The enhancement can be controlled by the CFJ size and strength. The downstream slot needs to be longer

due to having to counteract the momentum of the upstream CFJ set. Other configurations are studied to examine the effect of the slot size and the gap between the two CFJs. The final configuration with the gap of 0.5D between the two CFJ pairs, is the most effective to cancel out the side force.

Table 4: 3D Cylinder Resultant Force Coefficient Mach 0.45, 60° Sweep

Case	C_x	C_y	C_z	C_μ	P_c
Baseline	0.0650	0.0000	-0.0831	0.0	0.0
15% & 30% Span	0.0965	0.0017	-0.1847	0.05	0.02

III.D.3. Pitching Moment Generation

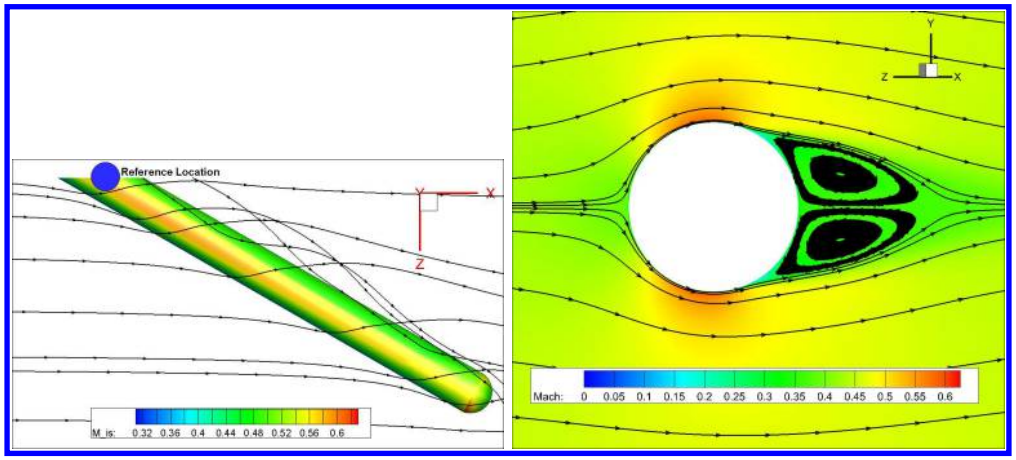

Figure 15: 3D Baseline Cylinder surface Mach contours, streamlines, and the flow around a cylinder cross section in the mid-span.

This section is to apply the configuration with side force cancellation in the previous section to a finite span cylinder with aspect ratio of 10. Figure 15 shows the configuration of the baseline finite span cylinder that is used as reference for the moment control study with the results listed in Table 5. Figure 15 shows that the baseline cylinder has two large counter-rotating vortices in the wake. The boundary conditions are mostly the same as those for the side force study with the exception that at the root of the cylinder a zero-gradient condition is imposed. This allows mass-flow in and out of that plane, permitting span-wise flow near the root of the cylinder. This is to mimic a potential windtunnel test configuration where the cylinder would not be mounted directly to the wall, but elevated on a sting. Symmetry boundary condition at the root was used initially, but prevented spanwise flow at the root and caused large flow separation. The tip of the cylinder is a hemisphere. No windtunnel wall is modeled. A far-field boundary extends 20 diameters from the cylinder tip. The moments are calculated around the pivot location at the root, marked by the blue circle. The moment directions are indicated by the XYZ coordinate system. The simulated Mach contours and streamlines of the CFJ cylinder with the counter injection CFJ are shown in Figure 16.

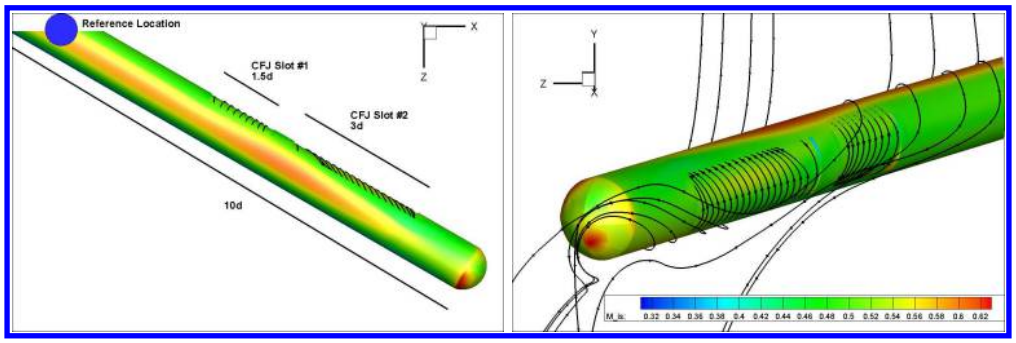

Figure 16: 3D Cylinder Diagram, 10d Span

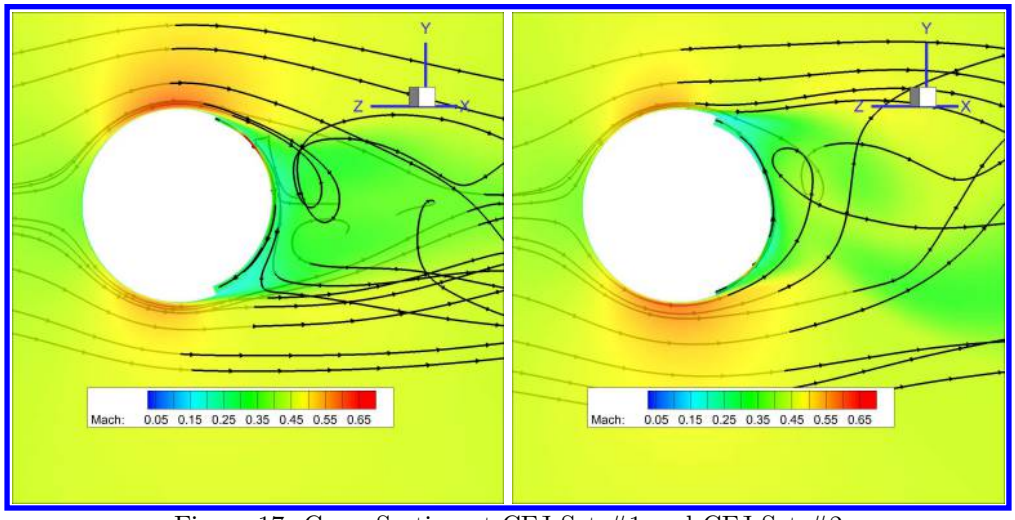

Figure 17: Cross Section at CFJ Set #1 and CFJ Set #2

As shown in Figure 17, the first CFJ set creates a region of high speed flow on the top of the cylinder. The streamlines of the CFJ 1 (Figure 17, left) shows that the jet is injected in the clockwise direction. It can be seen from the streamlines that the flow follows the contours of the cylinder without the separation shown in the baseline case of Figure 15. The larger, 2nd CFJ set shows the high speed flow on the bottom of the cylinder. This is because that the CFJ 2 is injected in the counter-clockwise direction as shown by the streamlines from the jet (Figure 17, right).

Table 5: 3D Cylinder Force and Moment Coefficients Mach 0.45, 60° Sweep

Type	P_c	$C_{\mu 1}$	$C_{\mu 2}$	C_x	C_y	C_z	C_{mx}	C_{my}	C_{mz}	C_F
3D-FS-CFJ-CY-1	0.0088	0.0500	0.025	0.1051	0.0086	-1.2546	-0.0163	-0.6111	0.0796	1.2590
3D-FS-CFJ-CY-2	0.0111	0.0667	0.025	0.1070	0.0018	-1.2566	-0.0748	-0.6247	0.1306	1.2612
3D-FS-CFJ-CY-3	0.0165	0.1000	0.025	0.1094	-0.0214	-1.2595	-0.1650	-0.6392	0.2896	1.2644
3D-FS-CFJ-CY-4	0.0141	0.1000	0.017	0.1073	-0.0367	-1.2561	-0.2077	-0.6121	0.3653	1.2612
Baseline	0.0000	0.0000	0.000	0.0793	0.0002	-1.1804	-0.0081	-0.4627	-0.0014	1.1831

Table 5 shows the resultant forces and moment coefficients of the cylinder in Figure 16. Ultimately, it is the pitching moment to control the motion of a refueling boom in the z-direction. Table 5 indicates that the CFJ cases are able to increase the pitching moment coefficient around the y-axis by nearly 50%. The increase in pitching moment is attributed to the substantially increased resultant force components: the magnitude of x and z force components. The Case 3D-FS-CFJ-CY-2 is the representative case for pitching moment control since it has the enhanced pitching moment and also the side force mostly canceled with C_Y of 0.0018.

The ultimate goal of this study is to vector the resultant force and associated moment, with the objective to have granular control authority about the pivot around the reference area, as indicated in Figure 16. This study indicates that using one CFJ set can have high lateral control authority and using two CFJ sets with counter-injecting direction can have high pitching control authority. The flight control using CFJ to replace the V-tail

IV. Conclusion

This study indicates that the flight control of 3D swept cylinder using CFJ for lateral and longitudinal motion control is feasible. Numerical simulation is conducted for a 3D cylinder with 60deg sweep angle, aspect ratio of 10, and freestream Mach number of 0.45. Applying one set of CFJ within a 15% span of the 3D cylinder is able to generate a very large side force coefficient of 3, which is more than sufficient for the cylinder lateral control. By using two sets of CFJ oriented in opposing injecting directions, the side

force can be canceled out, while enhancing the pitching moment for longitudinal control.

However, the study is just a initial step. More detailed CFJ and configurations design iteration are necessary with wind tunnel testing to validate the flight control features.

V. Acknowledgments

The simulations are conducted on Pegasus supercomputing system at the Center for Computational Sciences at the University of Miami. The research is partially supported by the AFOSR Summer Faculty Fellowship 2019 awarded to the third author.

Disclosure: Dr. GeCheng Zha is on the Board of Directors/Corporate Officer for CoFlow Jet and holds equity in CoFlow Jet. Dr. Zha is also the inventor of intellectual property licensed to CoFlow Jet.

References

[1] J.D. Anderson Jr. *Fundamentals of Aerodynamics*. McgGraw-Hill Eductation, 2010.

[2] Y. Yang and G.-C. Zha. Super Lift Coefficient of Cylinder Using Co-Flow Jet Active Flow Control. AIAA Paper-2018-0329, AIAA SciTech Forum 2018, 2018 AIAA Aerospace Sciences Meeting, Kissimmee, Florida, 8-12 January, 2018.

[3] G.-C. Zha and D. C. Paxton. A Novel Flow Control Method for Airfoil Performance Enhancement Using Co-Flow Jet. *Applications of Circulation Control Technologies*, Chapter 10, p. 293-314, Vol. 214, Progress in Astronautics and Aeronautics, AIAA Book Series, Editors: Joslin, R. D. and Jones, G.S., 2006.

[4] G.-C Zha and C. Paxton and A. Conley and A. Wells and B. Carroll. Effect of Injection Slot Size on High Performance Co-Flow Jet Airfoil. *AIAA Journal*, 43, 2006.

[5] G.-C. Zha and W. Gao and C. Paxton. Jet Effects on Co-Flow Jet Airfoil Performance. *AIAA Journal, No. 6*, 45:1222–1231, 2007.

[6] G.-C Zha and B. Carroll and C. Paxton and A. Conley and A. Wells. High Performance Airfoil with Co-Flow Jet Flow Control. *AIAA Journal*, 45, 2007.

[7] Wang, B.-Y. and Haddoukessouni, B. and Levy, J. and Zha, G.-C. Numerical Investigations of Injection Slot Size Effect on the Performance of Co-Flow Jet Airfoil . *AIAA Journal of Aircraft*, 45:2084–2091, 2008.

[8] B. P. E. Dano, D. Kirk, and G.-C. Zha. Experimental Investigation of Jet Mixing Mechanism of Co-Flow Jet Airfoil. AIAA Paper 2010-4421, 5th AIAA Flow Control Conference, Chicago, IL,, 28 Jun - 1 Jul 2010.

[9] B. P. E. Dano, G.-C. Zha, and M. Castillo. Experimental Study of Co-Flow Jet Airfoil Performance Enhancement Using Micro Discreet Jets. AIAA Paper 2011-0941, 49th AIAA Aerospace Sciences Meeting, Orlando, FL,, 4-7 January 2011.

[10] Lefebvre, A. and Dano, B. and Di Franzo, M. and Bartow, W. and Zha, G.-C. Performance of Co-Flow Jet Flow Airfoil with Variation of Mach Number. AIAA Paper 2013-0490, 51st AIAA Aerospace Science Meeting, Grapevine, TX, 7-10 Jan. 2013, to appear in Journal of Aircraft, 2016.

[11] Lefebvre, A. and Zha, G.-C. Numerical Simulation of Pitching Airfoil Performance Enhancement Using Co-Flow Jet Flow Control. AIAA Paper 2013-2517, 31st AIAA Applied Aerodynamics Conference, San Diego, CA, 24 - 27 June 2013.

[12] Lefebvre, A. and Zha, G.-C. . Design of High Wing Loading Compact Electric Airplane Utilizing Co-Flow Jet Flow Control. AIAA Paper 2015-0772, AIAA SciTech2015: 53nd Aerospace Sciences Meeting, Kissimmee, FL, 5-9 Jan 2015.

[13] Lefebvre, A. and Dano, B. and Bartow, W. and Di Franzo, M. and Zha, G.-C. Performance and Energy Expenditure of Co-Flow Jet Airfoil with Variation of Mach Number. *AIAA Journal of Aircraft*, 53:1757–1767, 2016.

[14] Liu, Z.-X. and Zha, G.-C. Transonic Airfoil Performance Enhancement Using Co-Flow Jet Active Flow Control. AIAA Paper 2016-3472, AIAA AVIATION 2016, 8th AIAA Flow Control Conference, Washington, D.C, June 13-17, 2016.

[15] Yang, Y.-C. and Zha, G.-C. Super-Lift Coefficient of Active Flow Control Airfoil: What Is the Limit? AIAA Paper 2017-1693, AIAA SCITECH2017, 55th AIAA Aerospace Science Meeting, Grapevine, Texas, 9-13 January 2017.

[16] Yang Y. Ren Y. McBreen B. Zha, G.-C. Super-Lift and Thrusting Airfoil of Coflow Jet Actuated by Micro-Compressors . AIAA Paper-2018-3061, AIAA AVIATION Forum 2018, 2018 Flow Control Conference, Atlanta, Georgia, June 25-29, 2018.

[17] P.R. Spalart and S.R. Allmaras. A One-equation Turbulence Model for Aerodynamic Flows. AIAA-92-0439, 1992.

[18] G.-C. Zha, Y. Shen, and B. Wang. An improved low diffusion E-CUSP upwind scheme . *Journal of Computer & Fluids*, 48:214–220, 2011.

[19] Y.-Q. Shen, B.-Y. Wang, and G.-C. Zha. Implicit WENO Scheme and High Order Viscous Formulas for Compressible Flows . AIAA Paper 2007-4431, 2007.

[20] B.-Y. Wang and G.-C. Zha. A General Sub-Domain Boundary Mapping Procedure For Structured Grid CFD Parallel Computation. *AIAA Journal of Aerospace Computing, Information, and Communication*, 5, No.11:2084–2091, 2008.

[21] Hu, Z.-J. PARALLEL COMPUTATION OF FLUID-STRUCTURAL INTERACTIONS USING HIGH RESOLUTION UPWIND SCHEMES. Ph.D. Thesis, University of Miami, Dept. of Mechanical and Aerospace Engineering, May 2005.

[22] Y.-Q. Shen and G.-C. Zha. Comparison of High Order Schemes for Large Eddy Simulation of Circular Cylinder Flow. AIAA-2009-0945, 47th AIAA Aerospace Sciences Meeting and Exhibit, Orlando, FL, Jan. 5-8, 2009.

[23] Y.-Q. Shen J.-Y. Gan and G.-C Zha. Comparison of Drag Prediction Using RANS models and DDES for the DLR-F6 Configuration Using High Order Schemes. 54th Aerospace Sciences Meeting, San Diego, CA, AIAA Paper 2016-0553, 2016.

[24] Y. Wang and G.-C. Zha. Study of Super-Lift Coefficient of Co-Flow Jet Airfoil and Its Power Consumption. AIAA Paper 2019-3652, AIAA Aviation 2019, AIAA Applied Aerodynamics Conference, Dallas, Texas, 17-21 June 2019.